# The identification of a partially coated dielectric medium from far field measurements‡

**Fioralba Cakoni[1], Gen Nakamura[2], Mourad Sini[3] and Noam Zeev[4]**

[1] Department of Mathematical Sciences, University of Delaware, Newark, Delaware 19716, USA.
[2] Department of Mathematics, Hokkaido University, Sapporo 060-0810, Japan.
[3] RICAM, Altenbergerstrasse 69, A 4040, Linz, Austria.
[4] Department of Mathematics and Statistics, Old Dominion University, Norfolk, VA 23529, USA

E-mail: `cakoni@math.udel.edu, mourad.sini@oeaw.ac.at, nzeev@odu.edu`

**Abstract.** We consider the two-dimensional electromagnetic inverse scattering problem for a dielectric medium partially coated with a thin layer of highly conductive material. Using the linear sampling method, we show that the approximate solution of the far field equation can be used to reconstruct the support of the coating in addition to the shape of the scattering obstacle. We also deduce formulas providing point-wise reconstruction of the surface conductivity on the coated portion and the real index of refraction on the uncoated portion of the boundary. Numerical examples are given for the case with constant surface conductivity and index of refraction showing the viability of our reconstruction procedure.

## 1. Introduction

We consider the scattering of time-harmonic electromagnetic waves with frequency $\omega$ by an inhomogeneous dielectric obstacle partially coated with a thin layer of a highly conductive material. This problem arises in nondestructive testing and underground interrogation.

In this work we restrict ourselves to the case where the scatterer is an infinitely long cylinder with axis in the $z$-direction and cross section $D$, and the incident electromagnetic field is a plane wave propagating in the direction the cylinder axis such that the electric field is polarized perpendicular to the z axis. We assume that the electric permittivity $\epsilon_0$ and magnetic permeability $\mu_0$ of the exterior background medium are positive constants whereas inside the cylindrical scatterer the magnetic permeability $\mu_0$ is the same as of the exterior medium but the electric permittivity $\epsilon$ is a positive function independent of $z$ and the conductivity $\sigma = 0$. The cross

‡ The research of F. Cakoni was supported in part by the U.S. Air Force Office of Scientific Research under Grant FA9550-05-1-0127.The research of M. Sini is supported by SFB 013 project.

section $D \subset \mathbb{R}^2$ is a bounded domain with $C^2$-boundary $\partial D$ such that the exterior domain $D_e := \mathbb{R}^2 \setminus \overline{D}$ is connected. We denote by $\nu$ the outward unit normal to $\partial D$. The boundary $\partial D = \overline{\partial D_t} \cup \overline{\partial D_c}$ is split into two open disjoint parts $\partial D_t$ and $\partial D_c$, where $\partial D_t$ corresponds to the uncoated part and $\partial D_c$ corresponds to the coated part of the surface of the scatterer. Let the positive function $\eta$ defined on $\partial D_c$ denote the surface conductivity which involves the physical parameters of the coating as well as its thickness. Assuming that the function $\eta$ does not depend on $z$, then the incident, interior and scattered magnetic fields have only one component in the $z$ direction, i.e. $H^i = (0,\ 0,\ U^i)$, $H^{int} = (0,\ 0,\ V)$ and $H^s = (0,\ 0,\ U^s)$, respectively. Eliminating the electric fields and denoting by $a(x) = \epsilon_0/\epsilon(x)$ the contrast, the direct scattering problem is formulated as the following transmission problem for $V$ and $U^s$ (see [3], [4]) .

$$\begin{cases} \nabla\cdot a(x)\nabla V + k^2\, V = 0 & \text{in} \quad D \\ \Delta U^s + k^2\, U^s = 0 & \text{in} \quad D_e \\ V - (U^s + U^i) = 0 & \text{on} \quad \partial D_t \\ V - (U^s + U^i) = -i\eta(x)\dfrac{\partial(U^s + U^i)}{\partial\nu} & \text{on} \quad \partial D_c \\ \dfrac{\partial V}{\partial\nu_a} - \dfrac{\partial(U^s + U^i)}{\partial\nu} = 0 & \text{on} \quad \partial D \\ \lim_{r\to\infty} \sqrt{r}\left(\dfrac{\partial U^s}{\partial r} - ikU^s\right) = 0, \end{cases} \tag{1}$$

where $r = |x|$, $U^i$ is the incident plane wave given by $U^i := e^{ikx\cdot d}$, $d \in \Omega := \{x : |x| = 1\}$,

$$\frac{\partial V}{\partial\nu_a}(x) := \nu(x)\cdot a(x)\nabla V(x), \qquad x \in \Gamma,$$

and the radiation condition in (1) holds uniformly with respect to $\hat{x} = x/|x|$.
In the following we assume that $a \in C^2(\overline{D})$ and $\eta \in C^2(\overline{\partial D_c})$ such that $a(x) \geq a_0 > 0$ for $x \in \overline{D}$ and $\eta(x) > \eta_0 > 0$ for $x \in \partial D_c$ (note that $\partial D_c$ is not necessarily connected). To formulate mathematically the direct scattering problem, we recall the usual Sobolev spaces $H^1(D)$, $H^1_{loc}(D_e)$ and $H^{\frac{1}{2}}(\partial D)$, and for $\partial D_c \subset \partial D$ we define by

$$H^{\frac{1}{2}}(\partial D_c) := \{u|_{\partial D_c} : u \in H^{\frac{1}{2}}(\partial D)\}$$
$$\tilde{H}^{\frac{1}{2}}(\partial D_c) := \{u \in H^{\frac{1}{2}}(\partial D_c) : \operatorname{supp} u \subseteq \overline{\partial D_c}\},$$

and denote by $H^{-\frac{1}{2}}(\partial D_c)$ and $\tilde{H}^{-\frac{1}{2}}(\partial D_c)$ the dual spaces $\left(\tilde{H}^{\frac{1}{2}}(\partial D_c)\right)'$ and $\left(H^{\frac{1}{2}}(\partial D_c)\right)'$, respectively, with $L^2$ as a pivot space (for details see [19]). For later use we also define the Hilbert space

$$\mathbb{H}^1(D, \partial D_c) := \left\{u \in H^1(D) \quad \text{such that} \quad \frac{\partial u}{\partial\nu} \in L^2(\partial D_c)\right\}$$

equipped with the usual graph norm

$$\|u\|^2_{\mathbb{H}^1(D,\partial D_c)} := \|u\|^2_{H^1(D)} + \left\|\frac{\partial u}{\partial\nu}\right\|^2_{L^2(\partial D_c)}.$$

The *forward scattering problem* reads: Given $D$, $a$, $\eta$ and $U^i$ as above, find $V \in H^1(D)$ and $U \in H^1_{loc}(D_e)$ that satisfy (1) where the boundary conditions are assumed in the sense of the trace operator. In [4] (see also [3]) it is shown that (1) has a unique solution depending continuously on the incident field. It is also known [13] that the radiating field $U^s$ have the asymptotic behavior

$$U^s(x) = \frac{e^{ikr}}{\sqrt{r}} U_\infty(\hat{x}, d) + O(r^{-3/2}), \quad r \to \infty \tag{2}$$

where $U_\infty(\hat{x}, d)$ is the *far field pattern* of the radiating solution $U^s$ which depends on the incident direction $d \in \Omega$ and the observation direction $\hat{x} \in \Omega$, where $\Omega$ is the unit circle.

The *inverse scattering problem* we are concern with is to determine the shape $D$, identify the uncoated part $\partial D_t$ and coated part $\partial D_c$ and reconstruct $\eta$ and $a|_{\partial D_t}$ from a knowledge of the far field pattern $U_\infty(\hat{x}, d)$ of the scattered field $U^s$ for $\hat{x}$, $d \in \Omega$. However we remark that, based on [5], the results of this paper hold true if $U_\infty(\hat{x}, d)$ is known on a limited aperture, i.e. for $d \in \Omega_0$ and $\hat{x} \in \Omega_1$, where $\Omega_1$ and $\Omega_0$ are open subsets of the unit circle $\Omega$. Note that, except for some reasonable regularity conditions (only for technical reasons) no a priori information is assumed. For the uniqueness of the support $D$ from the above data we refer the reader to [4] and [15] whereas uniqueness theorems for $\eta$ can be found in [4] and [8].

The solution of this inverse problem was first considered in [7] (see also [3]) where the linear sampling method was used to reconstruct the shape $D$ of a partially coated anisotropic dielectric with non smooth boundary. In addition, a variational method was given for determining the essential supremum of the surface conductivity $\eta$. The idea of [7] was further developed in [8] where $\eta$ is obtained as a solution of an integral equation. In the foundation of these approaches is the study of the so called the interior transmission problem that was first investigated in [6].

An alternative approach for solving the inverse scattering problem for partially coated perfect conductors was proposed in [9], [18] and [22] based on the probe and singular sources methods (see also [16], [17]) combined with asymptotical analysis of the Green's function related to the exterior mixed boundary value problem. A full reconstruction of the scattering objects including the shape, the support of the coating and the impedance coefficient it is presented in the above mentioned papers.

The goal of this paper is to extend the ideas of [18] and [22] to solve the inverse scattering problem for partially coated dielectrics using the linear sampling method. More precisely, we show that the approximate solution of the far field equation can be used to distinguish between the coated and uncoated boundary points, in addition to the reconstruction of the support of the scatterer. Furthermore, we obtain formulas that provide point-wise reconstruction of the index of refraction evaluated at the uncoated boundary points and the surface conductivity at the coated boundary points. The inversion scheme is essentially based on a detailed asymptotical analysis of the

Green's function associated with the interior transmission problem corresponding to our scattering problem which is developed in [21]. We note that the linear sampling method and the probe and singular source method use the far field data differently. However they have a common feature, namely whereas the linear sampling method is based on the behavior of Green's function of the interior problem corresponding to the scattering problem (in the current case interior transmission problem), the probe and singular source method rely on Green's function of the exterior problem. For a discussion on the probe and singular source method in comparison to the linear sampling we refer the reader to [16], [23], [25].

The plan of the paper is the following. In the next section we derive the solution algorithm for solving the inverse scattering problem. In order to avoid long and tedious calculations in our presentation, we state without proof some important results from [21] which are basic for the derivation of our reconstruction formulas. Section 3 is devoted to numerical implementation of the proposed algorithm where we present some numerical examples showing the viability of the method. Given the complexity of the inverse problem, the numerical study presented here is preliminary and by no means comprehensive and further investigation is necessary.

We conclude by saying that our reconstructing algorithm simply start by sampling the searching region and the information is built step by step from the reconstruction of the support till the reconstruction of the boundary coefficients. Parts of the algorithm can be used if more a-prior information is available.

## 2. The inverse scattering problem

The solution method for the inverse problem is based on the study of the approximate solution to the far field equation. To this end let us define the *far field operator* $F : L^2(\Omega) \to L^2(\Omega)$ by

$$Fg(\hat{x}) := \int_\Omega u_\infty(\hat{x}, d) g(d)\, ds(d), \qquad \hat{x} \in \Omega. \tag{3}$$

and the *far field equation*

$$(Fg)(\hat{x}) = G_\infty^{(j)}(\hat{x}, z) \qquad g \in L^2(\Omega), \hat{x} \in \Omega, \quad z \in \mathbb{R}^2, \quad j = 1, 2 \tag{4}$$

where $G_\infty^{(j)}(\hat{x}, z)$ is the far field pattern of

$$G^{(j)}(x, z) = \frac{\partial}{\partial x_j} \Phi(x, z), \qquad j = 1, 2,\ x = (x_1, x_2)$$

where $\Phi(x, z) := \frac{i}{4} H_0^{(1)}(k|x - z|)$ is the fundamental solution of the Helmholtz equation in $\mathbb{R}^2$ with $H_0^{(1)}$ being the Hankel function of the first kind of order zero. Typically the *linear sampling method* is based on the far field equation with the right hand side the far field pattern of the fundamental solution $\Phi(x, z)$ (see [3]). Here, we use on the right hand side of the far field equation the far field pattern of the derivative of the fundamental because we need singularities stronger than logarithmic to be able to

obtain the reconstruction formulas for $\eta$ and $a|_{\partial D_t}$.
As already known (see e.g. [3]), the study the far field equation (4) is related to the *interior transmission problem* refer to in following as (ITP)

$$\begin{aligned}
&\nabla\cdot a\nabla V_z^{(j)} + k^2\, V_z^{(j)} = 0 && \text{in } D\\
&\Delta W_z^{(j)} + k^2\, W_z^{(j)} = 0 && \text{in } D\\
&V_z^{(j)} - (W_z^{(j)} + G^{(j)}(\cdot, z)) = 0 && \text{on } \partial D_t\\
&V_z^{(j)} - (W_z^{(j)} + G^{(j)}(\cdot, z)) = -i\eta\, \frac{\partial}{\partial\nu}(W_z^{(j)} + G^{(j)}(\cdot, z)) && \text{on } \partial D_c\\
&\frac{\partial V_z^{(j)}}{\partial\nu_a} - \frac{\partial}{\partial\nu}(W_z^{(j)} + G^{(j)}(\cdot, z)) = 0 && \text{on } \partial D.
\end{aligned}$$

for $z \in D$ and $j = 1, 2$. The values of $k$ for which the homogeneous interior transmission problem (i.e. (ITP) with $G^{(j)}(\cdot, z) = 0$) has a non trivial solution, are called *transmission eigenvalues*. It is shown in [7] (see also [3]) that assuming that there exists a constant $\gamma > 0$ such that either $a \geq 1+\gamma$ or $0 < a_0 < a < 1-\gamma$ in $D$ and $k$ is not a transmission eigenvalue, then there exists a unique solution of (ITP) such that $V_z^{(j)} \in H^1(D)$ and $W_z^{(j)} \in \mathbb{H}^1(D, \partial D_c)$.

We recall the definition of a Herglotz wave function $v_g$ with kernel $g \in L^2(\Omega)$ which is an entire solution of the Helmholtz equation defined by

$$v_g(x) = \int_\Omega e^{ikx\cdot d} g(d)ds(d), \qquad x \in \mathbb{R}^2. \tag{5}$$

The following theorem is the bases of the linear sampling method and the proof can be found in [7] (see also Section 8.5 in [3]).

THEOREM 2.1 *Assume that $k$ is not a transmission eigenvalue, $a$, $\eta$ and $\partial D$ satisfy the assumptions stated in Section 1 and there exists a constant $\gamma > 0$ such that either $a \geq 1+\gamma$ or $0 < a_0 < a < 1-\gamma$ in $D$. Let $W_z^{(j)}, V_z^{(j)}$ be the unique solution of* (ITP). *Then*

*(i) For $z \in D$ and a given $\epsilon > 0$ there exists a $g_{z,\epsilon}^{(j)} \in L^2(\Omega)$ such that*

$$\|Fg_{z,\epsilon}^{(j)} - G_\infty^{(j)}(\cdot\,, z)\|_{L^2(\Omega)} < \epsilon$$

*and the corresponding Herglotz function $v_{g_{z,\epsilon}^{(j)}}$ converges in $\mathbb{H}^1(D, \partial D_c)$ to $W_z^{(j)}$ as $\epsilon \to 0$.*

*(ii) For a fixed $\epsilon > 0$, we have that*

$$\lim_{z\to\partial D} \|v_{g_{z,\epsilon}^{(j)}}\|_{\mathbb{H}^1(D,\partial D_c)} = \infty \quad \textit{and} \quad \lim_{z\to\partial D} \|g_{z,\epsilon}^{(j)}\|_{L^2(\Omega)} \to \infty.$$

*(iii) For $z \in \mathbb{R}^2 \setminus \overline{D}$ and a given $\epsilon > 0$, every $g_{z,\epsilon}^{(j)} \in L^2(\Omega)$ that satisfies*

$$\|Fg_{z,\epsilon}^{(j)} - G_\infty^{(j)}(\cdot\,, z)\|_{L^2(\Omega)} < \epsilon$$

*is such that*

$$\lim_{\epsilon\to 0} \|v_{g_{z,\epsilon}^{(j)}}\|_{\mathbb{H}^1(D,\partial D_c)} = \infty \quad \textit{and} \quad \lim_{\epsilon\to 0} \|g_{z,\epsilon}^{(j)}\|_{L^2(\Omega)} \to \infty.$$

An important remark is that, for $z \in D$, $v_{g^{(j)}_{z,\epsilon}}$ converges in $\mathbb{H}^1(D, \partial D_c)$ to $W^{(j)}_z$ as $\epsilon \to 0$. Therefore, since $v_{g^{(j)}_{z,\epsilon}}$ and $W^{(j)}_z$ satisfy the same Helmholtz equation in $D$, then from local regularity results for elliptic equations and interior estimates we have that $v_{g^{(j)}_{z,\epsilon}}(z)$ converges to $W^{(j)}_z(z)$ pointwisely for every $z \in D$.

Our main goal in the following is to show that $v_{g^{(j)}_{z,\epsilon}}$ with $g^{(j)}_{z,\epsilon}$ the approximate solution of (4) provided by Theorem 2.1, in the case when $z \in D$ approaches a point on $\partial D_c$ assumes different behavior from the case when $z \in D$ approaches a point on $\partial D_t$. A more detailed investigation of this solution reveals a connection between $v_{g^{(j)}_{z,\epsilon}}$ and the boundary coefficients $\eta$ and $a|_{\partial D_t}$. Since, $v_{g^{(j)}_{z,\epsilon}}$ approximates $W^{(j)}_z$ it suffices to study the behavior of $W^{(j)}_z$ where $W^{(j)}_z, V^{(j)}_z$ is the solution of (ITP). To this end, we need to recall some results established in [21]. For sake of presentation let us fix $j = 2$. Since $\partial D$ is a $C^2$-closed curve, we know that for every point $z_0 \in \partial D$ there exists a rigid transformation of coordinates under which $z_0$ is transformed to $0 := (0, 0)$ and in addition there exists a function $f \in C^2(-p, p)$ such that $f(0) = f'(0) = 0$ and $D \cap B(0, p) = \{(x, y) \in B(0, p);\ y < f(x)\}$. For a fixed point $z_0$, now we consider the new coordinative system by introducing the local coordinates transformation which takes $x$ to $\tilde{x} = T(x) = R(x) + M_{z_0}$, where $R$ is the rotation such that $R(\nu(z_0)) = (0, 1)$, and $M_{z_0}$ is the translation such that $M_{z_0} + R(z_0) = (0, 0)$. Simple calculations show that $R((0, 1)) = (-\nu_1(z_0), \nu_2(z_0))$ where $\nu_1(z_0)$ and $\nu_2(z_0)$ are the components of the normal vector to $\partial D$ at $z_0$. Let us set $\tau := R((0, 1))$. In the new coordinative system we denote by $\tilde{a}(\tilde{x}) = a(x)$ and $\tilde{\eta}(\tilde{x}) = \eta(x)$ for $x$ where they are defined. Let $a_0 = a(z_0)$ and $\eta_0 = \eta(z_0)$. Denoting by $\Gamma(x, z) = \frac{1}{2\pi} \ln \frac{1}{|x-z|}$ the fundamental solution of the Laplace equation, we consider the following problems

$$\begin{cases} \Delta \tilde{v}(\cdot, \tilde{z}) = 0 \text{ in } \mathbb{R}^2_- \\ \Delta \tilde{w}(\cdot, \tilde{z}) = 0 \text{ in } \mathbb{R}^2_- \\ \tilde{v}(\cdot, \tilde{z}) - \tilde{w}(\cdot, \tilde{z}) = \nabla \Gamma(\cdot,\ \tilde{z}) \cdot \tau \text{ on } \partial \mathbb{R}^2_- \\ a_0 \dfrac{\partial}{\partial \tilde{x}_2} \tilde{v}(\cdot, \tilde{z}) - \dfrac{\partial}{\partial \tilde{x}_2} \tilde{w}(\cdot, \tilde{z}) = \dfrac{\partial}{\partial \tilde{x}_2} \nabla \Gamma(\cdot,\ \tilde{z}) \cdot \tau \text{ on } \partial \mathbb{R}^2_-. \end{cases} \tag{6}$$

$$\begin{cases} \Delta \tilde{v}(\cdot, \tilde{z}) = 0 \text{ in } \mathbb{R}^2_- \\ \Delta \tilde{w}(\cdot, \tilde{z}) = 0 \text{ in } \mathbb{R}^2_- \\ \tilde{v}(\cdot, \tilde{z}) - (\tilde{w}(\cdot, \tilde{z}) + \nabla \Gamma(\cdot, \tilde{z}) \cdot \tau) = -i\eta_0 \dfrac{\partial}{\partial \tilde{x}_2} (\tilde{w}(\cdot, \tilde{z}) + \nabla \Gamma(\cdot,\ \tilde{z}) \cdot \tau) \text{ on } \partial \mathbb{R}^2_- \\ a_0 \dfrac{\partial}{\partial \tilde{x}_2} \tilde{v}(\cdot, \tilde{z}) - \dfrac{\partial}{\partial \tilde{x}_2} \tilde{w}(\cdot, \tilde{z}) = \dfrac{\partial}{\partial \tilde{x}_2} \left(\nabla \Gamma(\cdot,\ \tilde{z}) \cdot \tau\right) \text{ on } \partial \mathbb{R}^2_- \end{cases} \tag{7}$$

where $\tilde{x} = (\tilde{x}_1, \tilde{x}_2)$, $\tilde{z} = (\tilde{z}_1, \tilde{z}_2)$ and $\mathbb{R}^2_-$ is the half plane $\{\tilde{x} \in \mathbb{R}^2 :\ \tilde{x}_2 < 0\}$. For $x$ and $z$ near the point $z_0 \in \partial D$, let us define

$$w_z(x) := \tilde{w}(Tx, Tz) \qquad \text{and} \qquad v_z(x) = \tilde{v}(Tx, Tz). \tag{8}$$

The next theorem which is proven in [21] shows that $w_z$ is the dominant part of $W_z$ with respect to the singularity near $z_0$ where $W_z, V_z$ is the solution of (ITP).

THEOREM 2.2 *Let $z_0 \in \partial D$ and $x, z \in D$ are in the vicinity of $z_0$. Let $W_z, V_z$ be the unique solution of the interior transmission problem* (ITP) *for $j = 2$. Let $\tilde{w}(\cdot, \tilde{z}), \tilde{z}(\cdot, \tilde{z})$ satisfy (6) if $z_0 \in \partial D_t$ and (7) if $z_0 \in \partial D_c$ and $w_z$ is defined by (8). Then there exists a positive constant $C$ such that:*

*(i)* $|\mathrm{Re}(W_z - w_z)(x)| \leq C|\ln|z - z_0||$

*(ii)* $|\mathrm{Im}(W_z - w_z)(x)| \leq C$

Similar results can be stated if $G^1_\infty(\cdot, z)$ is used in the right hand side of the far field equation (4). Indeed, in the latter case we need to take the rotation transforming $\nu(z_0)$ to the vector $(1, 0)$ and state the problem in the half plane $\tilde{\mathbb{R}}^2_- := \{x \in \mathbb{R}^2 : x_1 < 0\}$. Obviously, in (6) and (7) $\partial/\partial\tilde{x}_2$ is replaced by $\partial/\partial\tilde{x}_1$. Before proceeding with our main result, we mention that the long technical proof of Theorem 2.2 is based on a detailed asymptotic analysis of Green's function associated with the interior transmission problem (ITP) which is also investigated in [21] (the latter is an important result on its own).

Now we are ready to state our main result which together with Theorem 2.1 provide the foundation of our reconstruction scheme.

THEOREM 2.3 *Assume that $k$ is not a transmission eigenvalue, $a$, $\eta$ and $\partial D$ satisfy the assumptions stated in Section 1 and there exists a constant $\gamma > 0$ such that $a \geq 1 + \gamma$ or $0 < a_0 < a < 1 - \gamma$ in $D$. Let $W^{(j)}_z, V^{(j)}_z$ be the solution of* (ITP) *and $\nu(z_0)$ be the outward normal vector at $z_0 \in \partial D$ . Then for $z \in D$ we have*

*(i)*
$$\lim_{z \to z_0} \frac{|\mathrm{Im}(W^{(j)}_z(z))|}{|\ln|(z - z_0) \cdot \nu||^s} = \begin{cases} 0 & \text{if } z_0 \in \partial D_t \\ \infty & \text{if } z_0 \in \partial D_c \end{cases} \quad \text{for} \quad s \in (0, 1) \tag{9}$$

*(ii)*
$$\eta(z_0) = \lim_{z \to z_0} \frac{-\nu_j(z_0) \ln|(z - z_0) \cdot \nu(z_0)|}{\pi \mathrm{Im}(W^{(j)}_z(z))} \qquad \text{for } z_0 \in \partial D_c \tag{10}$$

*(iii)*
$$\frac{a(z_0) - 1}{a(z_0) + 1} = \lim_{z \to z_0} \frac{\nu_j(z_0)}{4\pi \mathrm{Re}(W^{(j)}_z(z))(z - z_0) \cdot \nu(z_0)} \qquad \text{for } z_0 \in \partial D_t \tag{11}$$

*(iv)*
$$\nu(z_0) = \lim_{z \to z_0} \left( \pm \frac{\mathrm{Re}(W^{(1)}_z(z))}{\mathrm{Re}(W^{(2)}_z(z))} \sqrt{\frac{1}{1 + \left[\frac{\mathrm{Re}(W^{(1)}_z(z))}{\mathrm{Re}(W^{(2)}_z(z))}\right]^2}}, \pm \sqrt{\frac{1}{1 + \left[\frac{\mathrm{Re}(W^{(1)}_z(z))}{\mathrm{Re}(W^{(2)}_z(z))}\right]^2}} \right) \tag{12}$$

*and the sign is chosen so that $\nu(z_0)$ is oriented outside $D$.*

**Proof**: To proof the theorem we need to study the asymptotic behavior of $W^{(j)}_z$ for $z$ near a fixed point $z_0 \in \partial D$. To this end, we proceed in two steps. First we derive an explicit form of the solution of the transformed problems in the half plane. Then we combine these explicit formula with the results of Theorem 2.2 to compute $\eta(z_0)$ if $z_0 \in \partial D_c$ and $a(z_0)$ if $z_0 \in \partial D_t$.

*Step 1: The derivation of explicit formulas for $\tilde{w}$ and $\tilde{v}$.* Our goal at this point is to construct explicitly local solution to (6) and (7). To this end, for sake of presentation, in the following calculations we simply use $x = (x_1, x_2)$, $z = (z_1, z_2)$ instead of $\tilde{x} = (\tilde{x}_1, \tilde{x}_2)$ and $\tilde{z} = (\tilde{z}_1, \tilde{z}_2)$, respectively, and $w_z, v_z$ instead of the solutions $\tilde{w}(\cdot, \tilde{z}), \tilde{v}(\cdot, \tilde{z})$ to (6) and (7). However, at the end the final results will be formulated in terms of the original notations.

By linearity, it suffices to compute separately the solutions $v^{(j)}$ and $w^{(j)}$ (6) and (7) where $\nabla\Gamma(\cdot, \tilde{z}) \cdot \tau$ is replaced by $\partial x_j \Gamma(x, z)$ with $j = 1, 2$, respectively. We represent both $v_z^{(j)}$ and $w_z^{(j)}$ using the Poisson operators:

$$v_z^{(j)} := \frac{1}{2\pi} \int_{\mathbb{R}} e^{ix_1\xi + x_2|\xi|} \phi(\xi, z) d\xi \tag{13}$$

$$w_z^{(j)} := \frac{1}{2\pi} \int_{\mathbb{R}} e^{ix_1\xi + x_2|\xi|} \psi(\xi, z) d\xi. \tag{14}$$

Let us first consider $\partial_{x_2}\Gamma(x, z)$ and representing it as

$$\partial_{x_2}\Gamma(x, z) = -\frac{1}{4\pi} \int_{\mathbb{R}} e^{i(x_1 - z_1)\xi - (x_2 - z_2)|\xi|} d\xi \tag{15}$$

The following computations can be justified in a similar way as in [22].

First substituting (13), (14) and (15) in

$$v_z^{(2)} - w_z^{(2)} = \partial_{x_2}\Gamma(\cdot, z) \text{ for } x_2 = 0$$

implies that

$$\phi - \psi = -\frac{1}{2} e^{-iz_1\xi - z_2|\xi|}. \tag{16}$$

Substituting (13), (14) and (15) in

$$v_z^{(2)} - (w_z^{(2)} + \partial_{x_2}\Gamma(x, z)) = -i\eta \frac{\partial}{\partial x_2}(w_z^{(2)} + \partial_{x_2}\Gamma(\cdot, z)) \text{ for } x_2 = 0$$

yield

$$\frac{1}{2\pi} \int_{\mathbb{R}} e^{ix_1\xi} [\phi - \psi + \frac{1}{2} e^{-iz_1\xi - z_2|\xi|}] d\xi = -i\eta \frac{1}{2\pi} \int_{\mathbb{R}} |\xi| e^{ix_1\xi + z_2|\xi|} \psi + |\xi| e^{ix_1\xi + z_2|\xi| - iz_1\xi} \frac{1}{2} d\xi$$

which gives

$$\phi - \psi + \frac{1}{2} e^{-iz_1\xi - z_2|\xi|} = i\eta \left( -|\xi|\psi - \frac{|\xi|}{2} e^{-iz_1\xi + z_2|\xi|} \right)$$

and then

$$-(1 - i\eta|\xi|)\psi + \phi = -\frac{1}{2} (1 + i\eta|\xi|) e^{-iz_1\xi + z_2|\xi|}. \tag{17}$$

Similarly, from the second transmission condition in both (6) and (7)

$$a \frac{\partial}{\partial x_2} v_z - \frac{\partial}{\partial x_2} w_z = \frac{\partial}{\partial x_2} \frac{\partial}{\partial x_2} \Gamma(\cdot, z)$$

for $x_2 = 0$ we obtain that

$$(a\phi - \psi) = \frac{1}{2} e^{-iz_1\xi + z_2|\xi|}. \tag{18}$$

We first consider the solution of the problem (7). To this end, combining (17) and (18) we now have that

$$\psi = -\frac{1}{2}\frac{(a+1) + ia\eta|\xi|}{(1-a) + ia\eta|\xi|} e^{-iz_1\xi + z_2|\xi|}. \tag{19}$$

Substituting (19) in (14) gives

$$w_z^{(2)}(x) = -\frac{1}{4\pi}\int_{\mathbb{R}} \frac{(a+1) + ia\eta|\xi|}{(1-a) + ia\eta|\xi|} e^{i(x_1 - z_1)\xi + (x_2 + z_2)|\xi|} d\xi.$$

Hence, simple calculations shows that

$$\begin{aligned} w_z^{(2)}(z) = & -\frac{1}{4\pi}\int_{\mathbb{R}} \frac{(a+1) + ia\eta|\xi|}{(1-a) + ia\eta|\xi|} e^{2z_2|\xi|} d\xi \\ = & -\frac{a}{\pi}\int_0^{+\infty} \frac{e^{2z_2 r}}{(1-a) + ia\eta r} dr - \frac{1}{2\pi}\int_0^{+\infty} e^{2z_2 r} dr \\ = & -\frac{a}{\pi}\int_0^{+\infty} \frac{e^{2z_2 r}}{(1-a) + ia\eta r} dr + \frac{1}{4\pi z_2}. \end{aligned}$$

But we have that

$$\begin{aligned} \int_0^{+\infty} \frac{e^{2z_2 r}}{(1-a) + ia\eta r} dr &= \int_0^{\infty} \frac{(1-a) - ia\eta r}{(1-a)^2 + (a\eta)^2 r^2} e^{2z_2 r} dr \\ &= O(1) - i\int_0^{\infty} \frac{a\eta r}{(1-a)^2 + (a\eta)^2 r^2} e^{2z_2 r} dr. \end{aligned}$$

By straightforward computation we obtain that

$$\int_0^{\infty} \frac{a\eta r}{(1-a)^2 + (a\eta)^2 r^2} e^{2z_2 r} dr = O(1) - \frac{2}{a\eta}\ln(z_2).$$

Hence,

$$\begin{cases} \operatorname{Re} w_z^{(2)}(z) = \frac{1}{4\pi z_2} + O(\ln|z|), \text{ for } z \text{ near } 0 \\ \\ \operatorname{Im} w_z^{(2)}(z) = -\frac{1}{4\pi\eta}\ln(|z_2|) + O(1) \text{ for } z \text{ near } 0. \end{cases} \tag{20}$$

where $w_z^{(2)}, v_z^{(2)}$ solve (7) if $\nabla\Gamma(\cdot, \tilde{z}) \cdot \tau$ is replaced by $\partial x_2 \Gamma(x, z)$.

Next, we consider (6). Now, from (16) and (18), we have:

$$\phi(\xi, z) = \frac{1}{a-1} e^{-iz_1\xi + z_2|\xi|} \quad \text{and} \quad \psi(\xi, z) = \frac{1}{2}\frac{a+1}{a-1} e^{-iz_1\xi + z_2|\xi|}$$

By the same procedure as above we obtain that

$$w_z^{(2)}(x) = \frac{a+1}{4\pi(a-1)}\int_{\mathbb{R}} e^{i(x_1 - \tilde{z}_1)\xi + (x_2 + z_2)|\xi|} d\xi.$$

In particular, by simple calculation we obtain that

$$w_z^{(2)}(z) = \frac{a+1}{4\pi(a-1)} \int_0^\infty 2e^{2z_2 r} dr = \frac{a+1}{4\pi(a-1)z_2}, \tag{21}$$

where $w_z^{(2)}, v_z^{(2)}$ solve (6) if $\nabla\Gamma(\cdot, \tilde{z}) \cdot \tau$ is replaced by $\partial x_2 \Gamma(x, z)$.

Now we use $\partial_{x_1}\Gamma(x, z)$ and represent it as

$$\partial_{x_1}\Gamma(x, z) = i\frac{1}{4\pi} \int_{\mathbb{R}} e^{i(x_1-z_1)\xi-(x_2-z_2)|\xi|} \frac{\xi}{|\xi|} d\xi$$

Arguing as in the previous case we have that

$$\phi - \psi = i\frac{\xi}{2|\xi|} e^{-iz_1\xi - z_2|\xi|}, \tag{22}$$

$$-(1 - i\eta|\xi|)\psi + \phi = \frac{i}{2}[\frac{\xi}{|\xi|} + i\eta\xi]e^{-iz_1\xi+z_2|\xi|}, \tag{23}$$

and

$$(a\phi - \psi) = -\frac{i\xi}{2} e^{-iz_1\xi+z_2} \tag{24}$$

From (23) and (24) we obtain

$$\psi = \frac{1}{2} \frac{-a\eta|\xi| + i(a+1)}{(1-a) + ia\eta|\xi|} \frac{\xi}{|\xi|} e^{-iz_1\xi+z_2|\xi|}. \tag{25}$$

Plugging (25) in (14), we now have

$$w_z^{(1)}(x) = \frac{1}{4\pi} \int_0^\infty \frac{-a\eta + i(a+1)|\xi|}{(1-a) + ia\eta|\xi|} \frac{\xi}{|\xi|} e^{i(x_1-z_1)\xi+(x_2+z_2)|\xi|} d\xi$$

and hence

$$w_z^{(1)}(z) = \frac{1}{4\pi} \int_0^\infty \frac{-a\eta + i(a+1)|\xi|}{(1-a) + ia\eta|\xi|} \frac{\xi}{|\xi|} e^{2z_2|\xi|} d\xi$$

which means that $w_z^{(1)}(z) = 0$ where $w_z^{(1)}, v_z^{(1)}$ solve (7) if $\nabla\Gamma(\cdot, \tilde{z}) \cdot \tau$ is replaced by $\partial x_1 \Gamma(x, z)$. In a similar way it can be shown that

$$v_z^{(1)}(z) = 0 \tag{26}$$

where $w_z^{(1)}, v_z^{(1)}$ solve (6) if $\nabla\Gamma(\cdot, \tilde{z}) \cdot \tau$ is replaced by $\partial x_1 \Gamma(x, z)$.

Finally, from (20), the fact that $w_z^{(1)}(z) = v_z^{(1)}(z) = 0$ and the fact that $\nabla\Gamma(x, z)\cdot\tau = -\partial_{x_1}\Gamma(x, z)\nu_1(z_0) + \partial_{x_2}\Gamma(x, z)\nu_1(z_0)$, by going back to the original notations we obtain that

$$\begin{cases} \operatorname{Re} \tilde{w}(\tilde{z}, \tilde{z}) = \frac{\nu_2(z_0)}{4\pi\tilde{z}_2} + O(\ln|\tilde{z}|), \text{ for } \tilde{z} \text{ near } 0 \\ \\ \operatorname{Im} \tilde{w}(\tilde{z}, \tilde{z}) = -\frac{\nu_2(z_0)}{\pi\eta} \ln(|\tilde{z}_2|) + O(1) \text{ for } \tilde{z} \text{ near } 0 \end{cases} \tag{27}$$

where $\tilde{w}(\tilde{z}, \tilde{z})$ and $\tilde{v}(\tilde{z}, \tilde{z})$ is a solution of (7). Similarly, from (21) we obtain that

$$\tilde{w}(\tilde{z}, \tilde{z}) = \frac{(a+1)\nu_2(z_0)}{4\pi(a-1)\tilde{z} \cdot \nu_2(z_0)}. \tag{28}$$

where $\tilde{w}(\tilde{z},\tilde{z})$ and $\tilde{v}(\tilde{z},\tilde{z})$ is a solution of (7).

Obviously, in a similar way, in the case where the far field pattern of $G^{(1)}(x,z)$ is used on the right hand side of the far field equation instead of $G^{(2)}(x,z)$, we obtain the following formulas

$$\begin{cases} \operatorname{Re}\tilde{w}(\tilde{z},\tilde{z}) = \frac{\nu_1(z_0)}{4\pi\tilde{z}_1} + O(\ln|\tilde{z}|), \text{ for } \tilde{z} \text{ near } 0 \\ \\ \operatorname{Im}\tilde{w}(\tilde{z},\tilde{z}) = -\frac{\nu_1(z_0)}{\pi\eta}\ln(|\tilde{z}_1|) + O(1) \text{ for } \tilde{z} \text{ near } 0 \end{cases} \tag{29}$$

and

$$\tilde{w}(\tilde{z},\tilde{z}) = \frac{(a+1)\nu_1(z_0)}{4\pi(a-1)\tilde{z}\cdot\nu_1(z_0)}. \tag{30}$$

for the part $\tilde{w}(\tilde{z},\tilde{z})$ of the solution of (7) and (6), respectively.

*Step 2: Reconstruction of $\partial D_c$ and $\partial D_t$ parts of the known boundary $\partial D$ and formula for $\eta|_{\partial D_c}$ and $a|_{\partial D_t}$.* Having computed the explicit solution of the problems in half plane we are ready to prove the results of the theorem by using Theorem 2.2.

We proceed with the reconstruction of the support of the coating $\partial D_c$ and pointwise computation of $\eta|_{\partial D_c}$. To this end let $W_z^{(j)}$, $V_z^{(j)}$ $j=1,2$ be the unique solution of (ITP) corresponding to $G^{(j)}(x,z)$ for $j=1,2$, respectively. Transforming back (27) to the original local coordinative system near $z_0$, and using Theorem 2.2, we have that

$$\operatorname{Re}(W_z^{(j)}(z)) = \frac{\nu_j(z_0)}{4\pi(z-z_0)\cdot\nu(z_0)} + O(\ln|z-z_0|), \text{ for } z \text{ near } z_0 \tag{31}$$

$$\operatorname{Im}(W_z^{(j)}(z)) = -\frac{\nu_j(z_0)}{\pi\eta}\ln|(z-z_0)\cdot\nu(z_0)| + O(1), \text{ for } z \text{ near } z_0 \in \partial D_c \tag{32}$$

where $j=1,2$. Doing the same for (28), we have

$$\operatorname{Im}(W_z^{(j)}(z)) = O(1), \text{ for } z \text{ near } z_0 \in \partial D_t, \text{ for } j=1,2. \tag{33}$$

Hence from (32) and (33), we can distinguish $\partial D_c$ from $\partial D_t$ using the following criteria

$$\lim_{z\to z_0}\lim_{\epsilon\to 0}\frac{|\operatorname{Im}(v_{g_z^{j,\epsilon}}(z))|}{|\ln|(z-z_0)\cdot\nu||^s} = \begin{cases} 0 & \text{if } z_0 \in \partial D_t \\ \infty & \text{if } z_0 \in \partial D_c, \end{cases} \tag{34}$$

for every $s \in (0,1)$. Next, from (31), we obtain that

$$\lim_{z\to z_0}\frac{\operatorname{Re}(W_z^{(1)}(z))}{\operatorname{Re}(W_z^{(2)}(z))} = \frac{\nu_1(z_0)}{\nu_2(z_0)}.$$

Setting $t := \frac{\nu_1(z_0)}{\nu_2(z_0)}$ and using the relation $\nu_1(z_0)^2 + \nu_2(z_0)^2 = 1$ we have that $\nu_2(z_0) = \pm\sqrt{\frac{1}{1+t^2}}$ and therefore $\nu(z_0) = (\pm t\sqrt{\frac{1}{1+t^2}}, \pm\sqrt{\frac{1}{1+t^2}})$. hence we obtain the following formula for the normal vector in terms of $W_z^j$, for $j=1,2$

$$\nu(z_0) = \lim_{z\to z_0}\left(\pm\frac{\operatorname{Re}(W_z^{(1)}(z))}{\operatorname{Re}(W_z^{(2)}(z))}\sqrt{\frac{1}{1+\left[\frac{\operatorname{Re}(W_z^{(1)}(z))}{\operatorname{Re}(W_z^{(2)}(z))}\right]^2}}, \pm\sqrt{\frac{1}{1+\left[\frac{\operatorname{Re}(W_z^{(1)}(z))}{\operatorname{Re}(W_z^{(2)}(z))}\right]^2}}\right). \tag{35}$$

Note, that the sign is uniquely determined from the fact that the normal vector is oriented outward to the reconstructed boundary. Finally, from (32), we deduce that

$$\eta(z_0) = \lim_{z\to z_0} \frac{-\nu_j(z_0)\ln|(z-z_0)\cdot\nu(z_0)|}{\pi \mathrm{Im} W_z^{(j)}(z)}, \qquad j=1,2. \tag{36}$$

Finally we turn our attention to computing $a(z_0)$ for $z_0 \in \partial D_t$. From (28) by going back to the original local coordinative system near $z_0$ and using Theorem 2.2 we obtain that

$$\frac{a(z_0)-1}{a(z_0)+1} = \frac{\nu_2(z_0)}{4\pi \lim\limits_{z\to z_0} W_z^{(2)}(z)(z-z_0)\cdot\nu(z_0)}. \tag{37}$$

Similarly, using (30) we also have

$$\frac{a(z_0)-1}{a(z_0)+1} = \frac{\nu_1(z_0)}{4\pi \lim\limits_{z\to z_0} W_z^{(1)}(z)(z-z_0)\cdot\nu(z_0)}. \tag{38}$$

In particular, the slope of the normal vector can alternatively be computed by

$$\frac{\nu_1(z_0)}{\nu_2(z_0)} = \lim_{z\to z_0} \frac{W_z^{(1)}(z)}{W_z^{(2)}(z)}. \tag{39}$$

This ends the proof of the theorem. □

Combining Theorem 2.1 and Theorem 2.3 we established a procedure for solving the inverse problem. Let $g_{z,\epsilon}^{(j)} \in L^2(\Omega)$, $j=1,2$ be the approximate solution of the far field equation (4) given by Theorem 2.1 and let $v_{g_{z,\epsilon}^{(j)}}$ be the corresponding Herglotz function. If $W_z^{(j)}$, $V_z^{(j)}$ $j=1,2$ is the unique solution of (ITP), from Theorem 2.1 we have that for $z\in D$, $\lim_{\epsilon\to 0} v_{g_{z,\epsilon}^{(j)}(z)} = W_z^{(j)}(z)$. Using this in Theorem 2.3 we have the following reconstruction algorithm:

**The Reconstruction Algorithm**

(i) The boundary $\partial D$ can be characterized as the set of points $z\in\mathbb{R}$ where the $L^2(\Omega)$-norm of $g_{z,\epsilon}^{(j)}$ start to blow up.

(ii) Having reconstructed $\partial D$ the coated portion $\partial D_c$ can be distinguished from $\partial D_t$ using the following criteria

$$\lim_{z\to z_0}\lim_{\epsilon\to 0} \frac{|\mathrm{Im}(v_{g_z^{j,\epsilon}}(z))|}{\ln|(z-z_0)\cdot\nu|^s} = \begin{cases} 0 & \text{if } z_0\in\partial D_t \\ \infty & \text{if } z_0 \in \partial D_c, \end{cases} \qquad \text{for } z\in D \tag{40}$$

for every $s\in(0,1)$.

(iii) The surface conductivity $\eta$ on the coated part $\partial D_c$ can be computed by

$$\eta(z_0) = \lim_{z\to z_0} \frac{-\nu_j(z_0)\ln|(z-z_0)\cdot\nu(z_0)|}{\pi \lim_{\epsilon\to 0}\mathrm{Im}(v_{g_{z,\epsilon}^{(j)}}(z))}, \text{ for } z_0\in\partial D_c. \tag{41}$$

The index of refraction $a$ on the uncoated part $\partial D_t$ can be computed by

$$\frac{a(z_0)-1}{a(z_0)+1} = \frac{\nu_j(z_0)}{4\pi \lim_{z\to z_0} \lim_{\epsilon\to 0} \mathrm{Re}(v_{g^{(j)}_{z,\epsilon}}(z))(z-z_0)\cdot \nu(z_0)},\ z_0 \in \partial D_t. \tag{42}$$

The normal vector $\nu(z_0)$ is reconstructed by the following formula

$$\nu(z_0) = \lim_{\epsilon\to 0} \lim_{z\to z_0} \left( \pm \frac{\mathrm{Re}((v_{g^{(1)}_{z,\epsilon}}(z))}{\mathrm{Re}((v_{g^{(2)}_{z,\epsilon}}(z))} \sqrt{\frac{1}{1+\left[\frac{\mathrm{Re}((v_{g^{(1)}_{z,\epsilon}}(z))}{\mathrm{Re}((v_{g^{(2)}_{z,\epsilon}}(z))}\right]^2}}, \pm \sqrt{\frac{1}{1+\left[\frac{\mathrm{Re}((v_{g^{(1)}_{z,\epsilon}}(z))}{\mathrm{Re}((v_{g^{(2)}_{z,\epsilon}}(z))}\right]^2}} \right) \tag{43}$$

where the sign is appropriately chosen such that the normal vector is directed outward to the reconstructed boundary.

Remark 2.4 Note that (41) and (42) are justified assuming that $\nu^j(z_0) \neq 0$. Hence, since the boundary is not known a priori, in principle we need to solve the far field equation (4) for both cases of the right hand side $G^{(j)}_\infty(\cdot, z)$.

Remark 2.5 Theorem 2.1 in fact provides a characterization of the boundary from the behavior of $v_{g^{(j)}_{z,\epsilon}}$ in terms of a norm that depends on the unknown region $D$ and this can not be used in practice. Instead the linear sampling method characterizes the obstacle by the behavior of $g^{(j)}_{z,\epsilon}$. In practice, the approximate solution of the far field equation is obtained using the Tikhonov regularization combined with the Morozov discrepany principle. In general, an open question is whether this regularized solution behaves in the same way as $v_{g^{(j)}_{z,\epsilon}}$ given by Theorem 2.1. However, [1], [2] have mathematically justified that, in certain cases, applying a regular regularization technique to the far field equation leads to a solution $g$ that exhibits the desired behavior.

## 3. Numerical examples

In this section we shall present some numerical tests of the inversion scheme using synthetic far field data. For a given scatterer, the far field data is computed by using a cubic finite element code to approximate the near field and then employing a near to far field transformation [20] to compute the far field. The finite element computational domain is terminated by a rectilinear perfectly matched layer using a linear absorption function in the layer [10].

Having computed approximate values of the far field pattern at $N$ uniformly spaced points on the unit circle for $N$ incoming waves we have an $N \times N$ matrix $\mathcal{F}$ of approximate far field data

$$\mathcal{F}_{m,n} = u_{h,\infty}(d_m, d_n), \text{ where } d_m = (\cos(2\pi(m-1)/N, \sin(2\pi(m-1)/N)^\top$$

for $1 \leq m, n \leq N$, where $u_{h,\infty}$ is the finite element far field pattern. We add further noise to $\mathcal{F}_{m,n}$ to obtain

$$(\mathcal{F}_\epsilon)_{m,n} = \mathcal{F}_{m,n}(1+\epsilon\,\xi_{m,n})$$

where $\xi_{m,n}$ are complex numbers with real and imaginary part random numbers in $[-1, 1]$. In this study we choose $\epsilon = 0.02$. To set up the discrete version of the far field equation we need to compute the far field pattern $G_\infty^{(j)}(\hat{x}, z)$ of

$$G^j(x, z) = \frac{\partial}{\partial x_j} \frac{i}{4} H_0^{(1)}(k|x - z|) = -\frac{ik}{4} \frac{H_1^{(1)}(k|x - z|)}{|x - z|}(x_j - z_j), \qquad j = 1, 2.$$

Simple asymptotic analysis of the Hankel function $H_1^{(1)}$ as $|x| \to \infty$ shows that

$$G_\infty^{(1)}(\hat{x}, z) = i\sqrt{\frac{k}{8\pi}} \left(e^{-i(k\hat{x}\cdot z - 3\pi/4)}\right) \cdot \cos(\hat{x}), \quad G_\infty^{(2)}(\hat{x}, z) = i\sqrt{\frac{k}{8\pi}} \left(e^{-i(k\hat{x}\cdot z - 3\pi/4)}\right) \cdot \sin(\hat{x}).$$

For a given sampling point $z$, the discrete far field equation is then to compute $\vec{g} = (g_1, g_2, \ldots, g_N)$ such that

$$\mathcal{F}_\epsilon \vec{g} = \vec{b} \quad \text{where} \quad b_m = G_\infty^{(j)}(d_m, z), \qquad 1 \le m \le N. \tag{44}$$

This ill conditioned problem is solved approximately using the Tikhonov regularization and the Morozov discrepancy principle as described in [11]. The regularized solution $\vec{g} = (g_1, g_2, \ldots, g_N)$ of the far field equation and the corresponding Herglotz function are the basic ingredients of the reconstruction scheme as stated at the end of Section 2. The numerical study of this complex problem presented here is preliminary and by no mean comprehensive. There are open questions especially related to stability and the best implementation strategy, and more numerical experiments are needed.

We limit our discussion to two type of scatterers: a *disk* with radius $R = 0.4$ and an *ellipse* given by $x = 0.3\cos(s)$ and $y = 0.2\sin(s)$, $s \in [0, 2\pi]$. Both scatterers maybe uncoated, fully coated or partially coated. The index of refraction $a > 0$ inside the scatterer and the surface conductivity $\eta > 0$ are assumed to be constant as will become precise during the discussion. In all our examples we fix $k = 5$. Note that $a$ and $\eta$ depends on the frequency also.

### *3.1. Reconstruction of the support D*

We start by using the modified linear sampling method to approximate the boundary of the disk. Note that the difference of our approach from the standard linear sampling method is in the right hand side of the far field equation (4). We recall that for the reconstruction of $D$ one could use in the right hand side of (4) the far field pattern of the fundamental solution as in [7]. However, in order to recover $\eta$ and $a$ a more singular behavior of the imaginary part of the Herglotz function is needed. Having solved the far field equation for $g$, we compute $1/\|\vec{g}\|_{\ell^2}$ for $z$ on a uniform grid in the sampling domain. In the upcoming numerical results we have arbitrarily chosen $N = 61$, and we sample on a $101 \times 101$ grid on the square $[-1, 1] \times [-1, 1]$. In Figure 1 (a), (b) we have plotted the level curves $1/\|\vec{g}\|_{\ell^2} = C$ using the MATLAB contour command for the fully coated disk and ellipse both for $a = 1.5$ and $\eta = 0.2$. In Figure 2 (a), (b) and (c) we show the reconstruction of the ellipse partially coated on the lower part. One

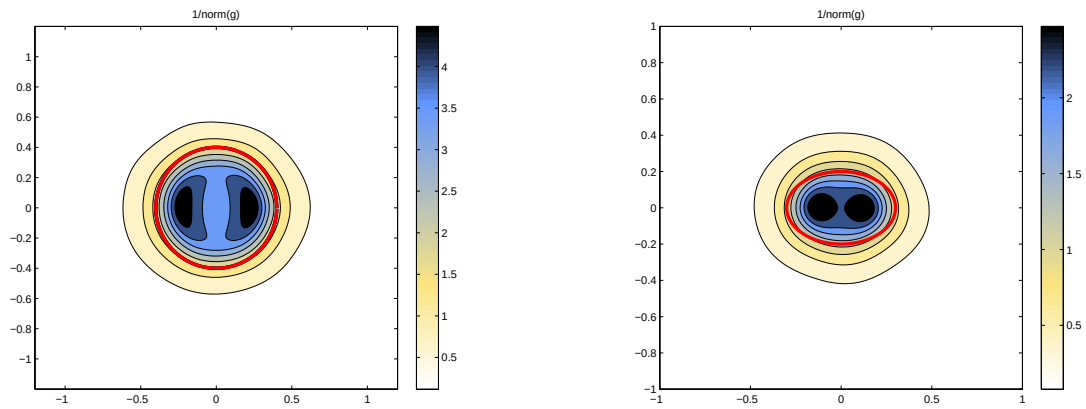


(a) (b)

**Figure 1.** Panel (a) shows the reconstruction of the fully coated disk. Panel (b) shows the reconstruction of the fully coated ellipse. In both $\eta = 0.2$ and $a = 1.5$ and red thick line indicates the true obstacle.

observes the enhancing scattering effect of the thin conducting coating. In particular in the panel (c), although the contrast $1 - a = 0.1$ is very small, the lower part of the ellipse is still visible due to the presence of the coating. Note that if $\eta$ is large enough (how large depends on the frequency and the skin depth) the coating portion behaves as a perfect conductor.

### *3.2. Reconstruction of the normal vector on $\partial D$*

Having computed the regularized solution of (44) we have a discrete level set function $1/\|\vec{g}\|_{\ell^2}$. Choosing a contour value $C$ then provides a reconstruction of the boundary $\partial D$ of the scatterer. Obviously, the choice of $C$ is very important. Up to date there is no mathematical criteria how to choose $C$ and in general an ad-hoc procedure is implemented. Usually, the chosen $C$ is picked by

$$C = \theta(\max_z(1/\|\vec{g}\|)) + (1-\theta)(\min_z(1/\|\vec{g}\|))$$

for some $0 < \theta < 1$. For an appropriate choice of $C$, the boundary points are the points $z$ on the grid such that $1/\|\vec{g}\| = C$. For each point in the set of (reconstructed) boundary points we can now use (43) to evaluate the outward normal vector to the boundary. This is an important step of the algorithm since the normal vector appears in the reconstruction formula for $a$ and $\eta$. In Figure 3, we show our results on normal reconstruction for the case of the fully coated ellipse with $a = 1.5$ and $\eta = 0.2$.

### *3.3. Detecting boundary coatings*

Next we test (40) which provides a criteria to distinguish between a coated and uncoated part of the boundary of the dielectric medium. This needs the evaluation of the Herglotz

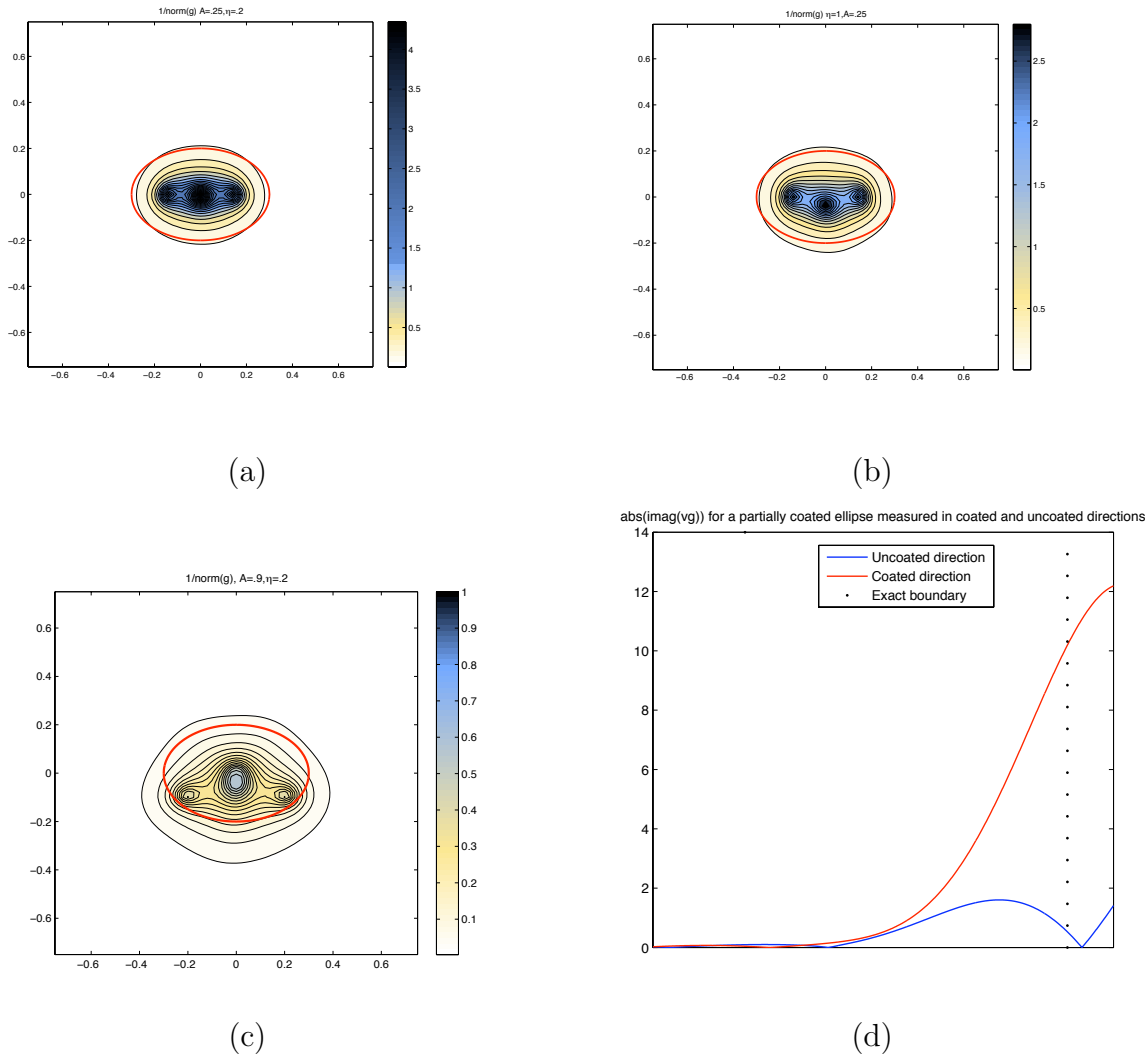


**Figure 2.** Panel (a) shows the reconstruction of the partially coated (on the lower half) ellipse with $a = 0.25$ and $\eta = 0.2$. Panel (b) shows the reconstruction of the partially coated (on the lower half) ellipse with $a = 0.25$ and $\eta = 1$. Panel (c) shows the reconstruction of the partially coated (on the lower half) ellipse with $a = 0.9$ and $\eta = 0.2$. The graph in panel (d) shows the behavior of $|\mathrm{Im}(v_{g_z^{(2)}}(z))|$ at the coated and uncoated boundary points for the ellipse reconstructed in panel (b). In particular, the solid blue graph shows a plot of $|\mathrm{Im}(v_{g_z^{(2)}}(z))|$ as $z$ approaches the point $(0, 0.2)$ (on the uncoated part) in the vertical direction whereas the dash red graph shows a plot $|\mathrm{Im}(v_{g_z^{(2)}}(z))|$ as $z$ approaches the point $(0, -0.2)$ (on the coated part) in the vertical direction

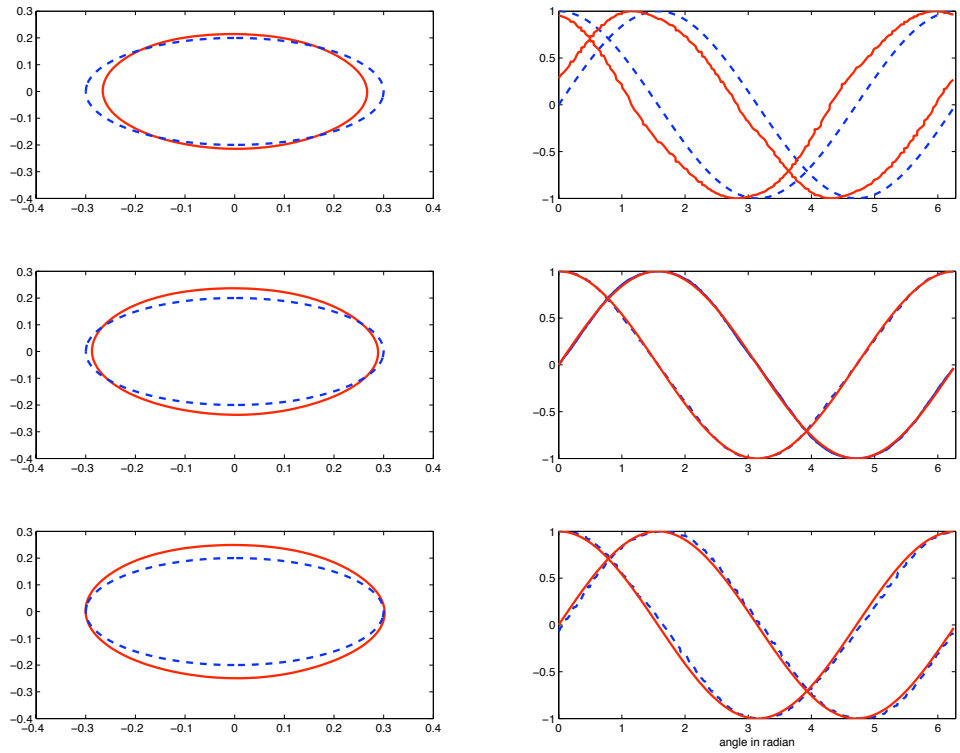


**Figure 3.** The right plots show the reconstruction of both components of the outward unit normal vector to the ellipse reconstructed in Figure 1 (b). The reconstructed normal components are presented by the red solid graphs. The blue dash graphs show the correct normal vector. We use the reconstructed boundary points which lie on the level curve presented by the red solid line on the corresponding left plot. The dash blue line on the left plots denotes the exact boundary. The respective $L^2$-error for the normal reconstruction in each of the three cases is 3.338, 0.1971 and 0.7445. In the two bottom cases, the exact normal vector and the reconstructed one are almost indistinguishable.

function $v_{g_z}$, having available the kernel $\vec{g}$ at $N$ points on the unit circle. This task is done by using Rieman sums with $N$ colocation points. Panel (d) in Figure 2 shows the behavior of $|\mathrm{Im}(v_{g_z^{(2)}}(z))|$ as $z$ goes through the uncoated boundary point (0, 0.2) and coated boundary point (0, −0.2) of the partially coated ellipse reconstructed in Figure 2(b). One observes the behavior predicted by (40). In Figure 4 we show plots of $|\mathrm{Im}(v_{g_z}(z))|$ for sampling points $z$ in the grid in the case of the disk. In particular, panel (a) corresponds to the plot of $|\mathrm{Im}(v_{g_z^1}(z))|$ for the fully coated disk. In this case, as discussed in Remark 2.4, no information is obtained near points where $\nu_1 = 0$. Thus both $|\mathrm{Im}(v_{g_z^1}(z))|$ and $|\mathrm{Im}(v_{g_z^2}(z))|$ need to be considered and this is done in the plot shown in panel (b). Panel (c) instead, corresponds to the case of the uncoated disk, therefore $|\mathrm{Im}(v_{g_z}(z))|$ remains very small near the boundary.

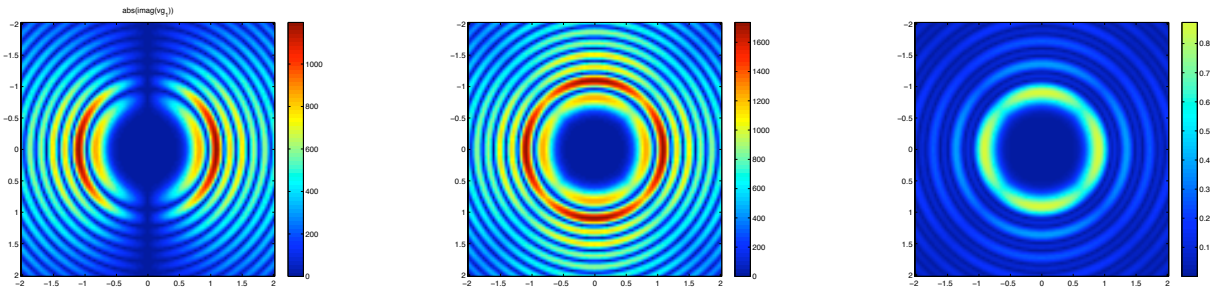


(a) (b) (c)

**Figure 4.** Panel (a) shows a plot of $|\mathrm{Im}(v_{g_z^{(1)}}(z))|$ for the coated disk with $a = 1.5$ and $\eta = 1$. Panel (b) shows a plot of $|\mathrm{Im}(v_{g_z^{(1)}}(z))| + |\mathrm{Im}(v_{g_z^{(2)}}(z))|$ for the coated disk with $a = 1.5$ and $\eta = 1$. Panel (c) shows a plot of $|\mathrm{Im}(v_{g_z^{(1)}}(z))| + |\mathrm{Im}(v_{g_z^{(2)}}(z))|$ for the uncoated disk with $a = 1.5$.

### *3.4. Reconstruction of a*

Having reconstructed the shape and the normal vector together with the support of the coating, we now use (42) to recover the index of refraction on the uncoated part of the boundary. In the current examples we reconstruct the constant index of refraction $a$ of an homogeneous isotropic medium. This constant $a$ is estimated by

$$\frac{a-1}{a+1} \approx \lim_{z \to z_0} \frac{\nu_j(z_0)}{4\pi \mathrm{Re}(v_{g_z^{(j)}}(z))(z - z_0) \cdot \nu(z_0)}, \; j = 1, 2 \tag{45}$$

where $z_0$ is any point on the uncoated part of the boundary and $v_{g_z}(z)$ is computed as explained in Section 3.3. We remark that the implementation of (45) suffers an additional numerical instability due to the fact that in practice $\mathrm{Re}(v_{g_z}(z))$ becomes finitely large near the boundary whereas $(z - z_0) \cdot \nu(z_0)$ is infinitely large. This instability issue requires further numerical study. In the current numerical investigation we deal with it in an ad-hoc manner, namely by truncating the power series expansion of $1/(z - z_0) \cdot \nu(z_0)$. In particular, in the upcoming examples we consider 10 terms in the power series (this can also be seen as a sort of regularization by truncation!). Reconstructions for the disk shown in Figure (5) (a) are done by letting $z$ approach $z_0 = (0.4795, 0)$ (note that the exact boundary point is $(0.4, 0)$) in the horizontal direction, thus we use $\nu_1$ in the formula. However, we obtain quite similar results by approaching the boundary points in the radial direction, since the isolines $1/\|\vec{g}\| = C$ are almost circles. The results for the ellipse presented in Figure 5 (b) are computed by approaching the (reconstructed) boundary point $z_0 = (0.3495, 0)$ (the exact boundary point is $(0.3, 0)$) in the horizontal direction. In both examples, the results become worse as $|a - 1|$ increases meaning as the scatterer becomes stronger.

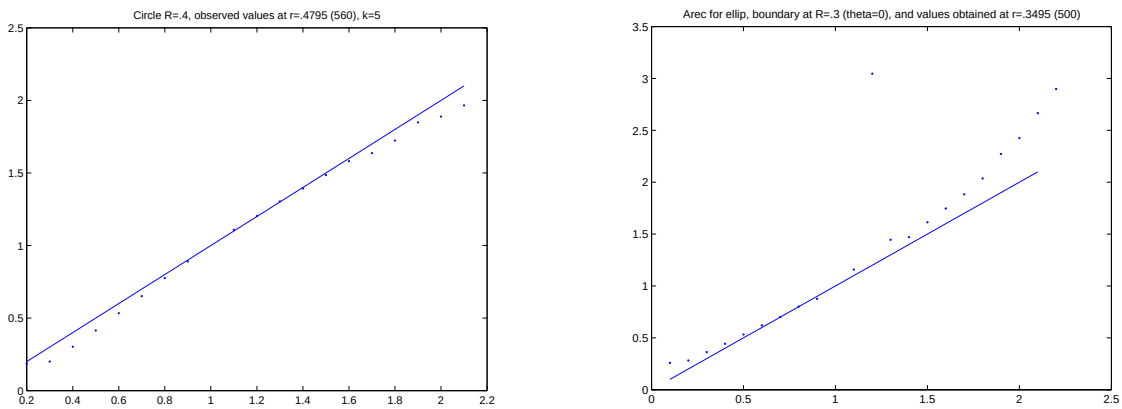


(a) (b)

**Figure 5.** Panel (a) shows the reconstruction of a range of $a$ for the uncoated disk. Panel (b) shows the reconstruction of a range of $a$ for the uncoated ellipse. The dots represent the reconstructed value of $a$ versus the exact value. An exact reconstruction would lie on the solid line.

### *3.5. Reconstruction of $\eta$*

Using (41) it is now possible to estimate pointwise the surface conductivity $\eta$ on the coated part of the boundary. In particular, in this numerical study the constant conductivity is approximated by

$$\eta \approx \lim_{z \to z_0} \frac{-\nu_j(z_0) \ln |(z - z_0) \cdot \nu(z_0)|}{\pi \mathrm{Im}(v_{g_z^{(j)}}(z))}, \; j = 1, 2 \tag{46}$$

where $z_0$ is any point on the coated part of the boundary. Numerical results for the fully coated disk and the fully coated ellipse are shown in Figure 6 (a) and (b), respectively. In the case of the disk we take the exact boundary point $z_0 = (0.4, 0)$, whereas in the case of the ellipse we take $z_0 = (0.3745, 0)$ (the exact boundary point would be $(0.3, 0)$). Similar to Section 3.4, in (46), we replace $\nu_j(z_0) \ln |(z - z_0)|$ by 10 terms in its power series expansion. In general, the reconstruction of large $\eta$ are worse since large $\eta$ correspond to thick impenetrable coatings. This fact was also observed in [7]. As a heuristic possible way to improve the reconstruction due instability, we suggest a kind of post processing of the reconstruction results. More precisely, one could scale reconstructed values of $\eta$ with an appropriate fixed constant chosen by correcting one value of $\eta$ synthetically simulated for a given shape, coating support and $a$. The plot in Figure 7 is a scaled version of the plot in Figure 6 (b) where we have corrected the value of $\eta = 0.1$.

Finally, for the partially coated (on the lower half) ellipse we used (45) and (46) to reconstruct both $\eta$ and $a$. The results for several combinations of $\eta$ and $a$ are shown in the table in Figure 7

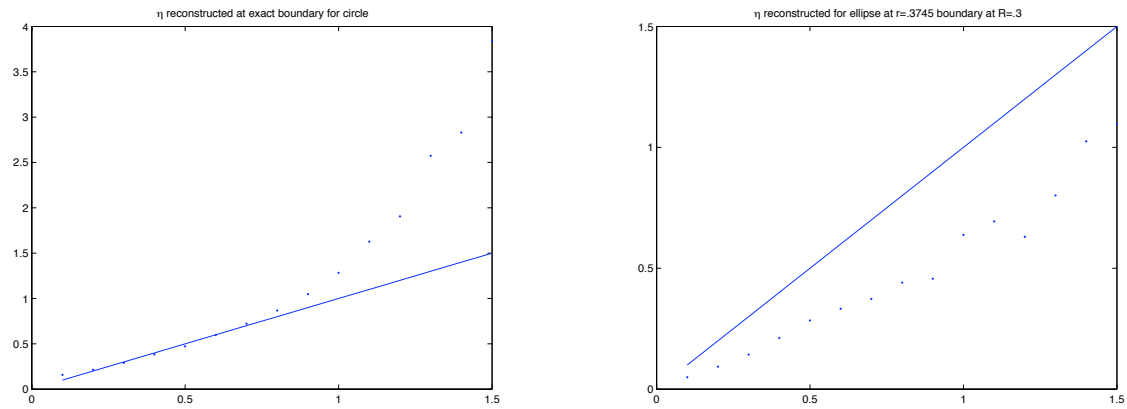


(a) (b)

**Figure 6.** Panel (a) (panel (b)) shows the reconstruction of a range of $\eta$ for the fully coated disk (fully coated ellipse) using $z_0 = (0.4, 0)$ ($z_0 = (0.3745, 0)$). The dots represent the reconstructed value of $\eta$ versus the exact value. An exact reconstruction would lie on the solid line. Here $a = 1.5$.

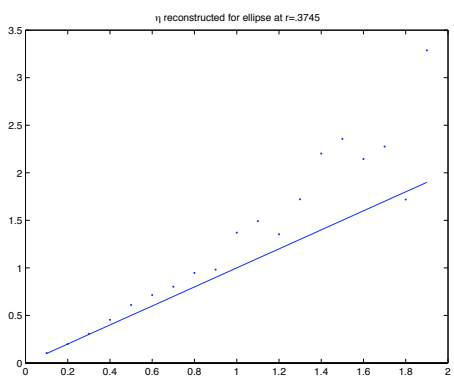


| Exact $\eta$, $a$ | Reconstructed $\eta$, $a$ |
|---|---|
| 0.1, 1.1 | 0.2204, 1.1407 |
| 0.1, 1.5 | 0.1727, 1.9848 |
| 0.2, 1.5 | 0.2892, 1.8904 |
| 1, 1.5 | 1.3147, 1.8601 |

**Figure 7.** The graph shows the corrected reconstruction of the values of $\eta$ for the fully coated ellipse presented in Figure 6 using an appropriate scaling constant. The table shows reconstructed values of $\eta$ and $a$ for the partially coated ellipse.

## Acknowlegment

The research of F. Cakoni is supported in part by the U.S. Air Force Office of Scientific Research under Grant FA9550-05-1-0127. The research of M. Sini is supported by SFB 013 project. The support is gratefully acknowledge.

## References

[1] Arens T 2004 Why linear sampling method works *Inverse Problems* 20 163-173.
[2] Arens T and Lechleiter A The linear sampling method revisited, *J. Integral Equations and Applications* (accepted).

[3] Cakoni F and Colton D 2006 *Qualitative Methods in Inverse Scattering Theory. An introduction.* Interaction of Mechanics and Mathematics, Springer.

[4] Cakoni F and Colton D 2003 A uniqueness theorem for an inverse electomagnetic scattering problem in inhomogeneous anisotropic media *Proc. Edinburgh Math. Soc.* 46 293-314.

[5] Cakoni F and Colton D 2003 Combined far field operators in electromagnetic inverse scattering theory *Math. Methods Appl. Sci.* 26 413-429.

[6] Cakoni F , Colton D and Haddar H 2002 The linear sampling method for anisotropic media *J. Comput. Appl. Math.* 146 285-299.

[7] Cakoni F, Colton D and Monk P 2005 The determination of the surface conductivity of a partially coated dielectric *SIAM. J. Appl. Math.* 65 767-789.

[8] Cakoni F, Colton D and Monk P, The determination of boundary coefficients from far field measurements (to appear).

[9] Cheng J, Liu J J and Nakamura G 2003 Recovery of the shape of an obstacle and the boundary impedance from the far-field pattern, *J. of Maths of Kyoto University* 43 No.1 165-186.

[10] Collino F and Monk P 1998 The Perfectly Matched Layer in curvilinear coordinates *SIAM J. Sci. Comput.* 19 2061-2090.

[11] Colton D, Piana M and Potthast P 1997 A simple method using Morozov's discrepancy principle for solving inverse scattering problems, *Inverse Problems* 13 1477-1493.

[12] Colton D and Kress R 2006 Using fundamental solutions in inverse scattering Inverse Problems 22 No. 3 R49–R66.

[13] Colton D and Kress R 1998 *Inverse Acoustic and Electromagnetic Scattering Theory.*, 2nd ed., Springer Verlag

[14] Colton D, Päivärinta L and Sylvester J 2007 The interior transmission problem *Inverse Problems and Imaging* 1 13-28.

[15] Hähner P 2000 On the uniqueness of the shape of a penetrable, anisotropic obstacle *J. Comput. Appl. Math.* 116 167-180.

[16] Honda H, Nakamura G, Potthast R and Sini M 2008 The no-response approach and its relation to non-iterative methods for the inverse scattering *Ann. Math. Pura. Appl* 187 1 7-37.

[17] Ikehata M 1998 Reconstruction of the shape of the inclusion by boundary measurements *Comm. PDE* 23 1459-1474.

[18] Liu JJ, Nakamura G and Sini M 2007 Reconstruction of the shape and surface impedance from acoustic scattering data for arbitrary cylinder *SIAM. J. Appl. Math* 67 4 1124-1146.

[19] McLean W 2000 *Strongly Elliptic Systems and Boundary Integral Equations.* Cambridge University Press.

[20] Monk P and Süli E 1998 The adaptive computation of far field patterns by a posteriori error estimation of linear functionals *SIAM J. Numer. Anal.* 36 251-274.

[21] ..... , Asymptotical behavior of Green's function of the interior transmission problem *RICAM preprint*

[22] Nakamura G and Sini M 2007 Obstacle and boundary determination from scattering data *SIAM. J. Math. Anal* 39 3 819-837.

[23] Nakamura G, Potthast R and Sini M 2006 Unification of the probe and singular sources methods for the inverse boundary value problem by the non-responce test *Comm. PDE* 31 10 1505-1528.

[24] Potthast R 2001 *Point Sources and Multipoles in Inverse Scattering Theory*, Research Notes in Mathematics, Vol.427, Chapman-Hall/CRC, Boca Raton FI.

[25] Potthast R 2006 A survey on sampling and probe methods for inverse problems *Inverse Problems* 22 2 R1-R47.